Link analysis of a deformable mirror device based optical crossbar switch

Robert W. Cohn,* MEMBER SPIE
Texas Instruments Incorporated
Central Research Laboratories
Dallas, Texas 75265

Abstract. An optical crossbar switch is proposed that uses a semiconductor-addressed, deformable-mirror spatial light modulator to direct gigabit-per-second optical transmissions to several receivers. The switch performance is described in terms of size, number, and deflection range of micromechanical mirror elements, as well as emitter, detector, and lens dimensions. These parameters are incorporated in a link energy budget and estimates of system dimensions. Maximum-sized 128- to 1000-channel crossbars appear feasible based on current and projected performance limits of various lightwave components.

Subject terms: spatial light modulators; deformable mirror; optical crossbar switch; link analysis.

Optical Engineering 31(1), 134–140 (January 1992).

1 Introduction

Reconfigurable crossbar interconnection networks that support high-rate data communications are essential components in a variety of applications including parallel processing computer architectures,[1,2] telecommunications switching systems,[3] and avionics busses. Optical systems can be developed in which a few lenses perform one-to-many and many-to-one mappings and a spatial light modulator (SLM) is used as a programmable binary switch matrix. The optical crossbar switch (Fig. 1) connects N optical transmitters to N optical receivers. Any mapping of inputs to outputs is possible including 1 to N broadcasting and N to 1 combining. Light from individual sources is spread across individual rows of an SLM. Light from all transmitting pixels in a column is collected by a single receiver. Receiver j is connected to transmitter i when the SLM pixel in row i, column j, is in the transmitting state.

Optical crossbar switches can support high-rate optical data transmissions provided lightwave components perform adequately and signal loss and degradation are not too great. Large interconnectivity optical crossbar switches are known to be inefficient in transmitting light energy.[4] The uniform broadcast of any transmitted channel to N elements of an SLM ideally reduces per channel efficiency to $1/N$. In the deformable mirror device (DMD) switched crossbar proposed here, additional losses arise because small-area diodes are required to detect gigabit-per-second rate signals. In demagnifying the image of the DMD onto a detector, losses proportional to $1/N$ are expected because imaging lenses are necessarily limited in numerical aperture (NA). A link analysis will be developed that includes NA and aperture sizes of the critical optical components, as well as crosstalk arising from the finite contrast ratio of the DMD. The crossbar configuration and analysis will be developed in light of the performance of available and anticipated lightwave components.

2 System Description

Figure 2 shows the open-air portion of the crossbar. The image reflected off the DMD is reimaged onto a sampling mask, which is used to block out light from the areas between the deflectable elements of the DMD. Shadow masking provided good contrast for a reflective membrane SLM of similar dimensions to current DMDs.[5]

The deformable mirror SLM (Fig. 3) is an array of discrete mirror elements. When voltage is applied to a field plate, the mirror element, which is suspended over an air gap, will deflect. A semiconductor-addressing circuit underlies the mirror structure to allow total flexibility in driving individual DMD pixels.[6] In the crossbar, a deflected mirror element reflects light away from the optical axis for an off state while an on state results when the element is undeflected.

The crossbar may be viewed as a communications link consisting of transmitter, receiver, and the transmission medium (Fig. 4). The transmission medium includes short lengths of optical fiber and open-air optics. The significant link loss

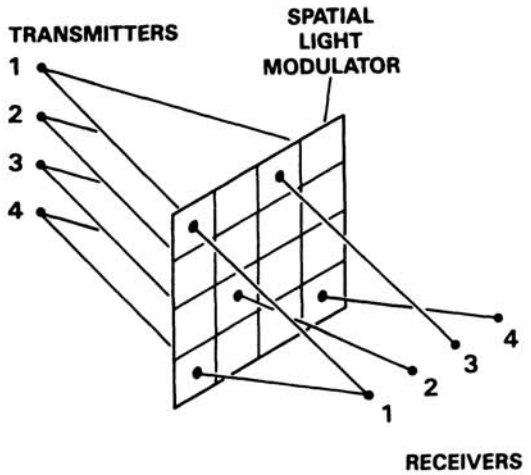

Fig. 1 Conceptual optical crossbar switch.

*Current affiliation: University of Louisville, Department of Electrical Engineering, Louisville, Kentucky, 40292.

Paper 3000 received Oct. 15, 1990; accepted for publication Aug. 6, 1991. This paper is a revision of a paper presented at the SPIE conference on Spatial Light Modulators and Applications II, August 1987, San Diego, Calif. The paper presented there appears (unrefereed) in SPIE Proceedings Vol. 825.

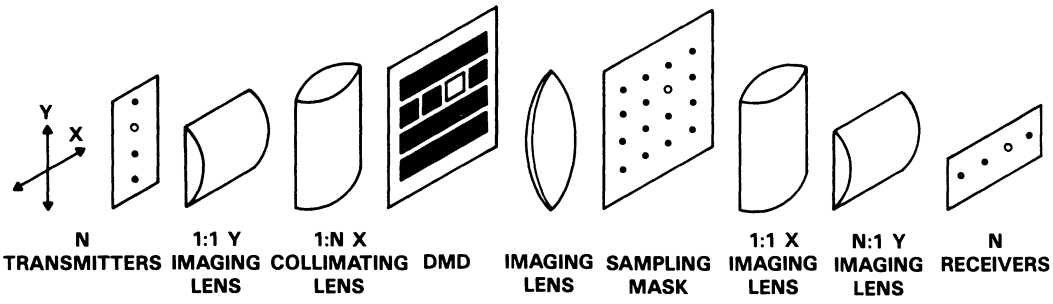

Fig. 2 Proposed optical crossbar switch (unfolded view; the DMD is actually a reflective modulator used with a beamsplitter). The figure illustrates the interconnection of the second transmitter row to the third receiver column by deflecting all pixels except the on (unshaded) pixel. The beamsplitter for the DMD and image inversions are omitted for clarity.

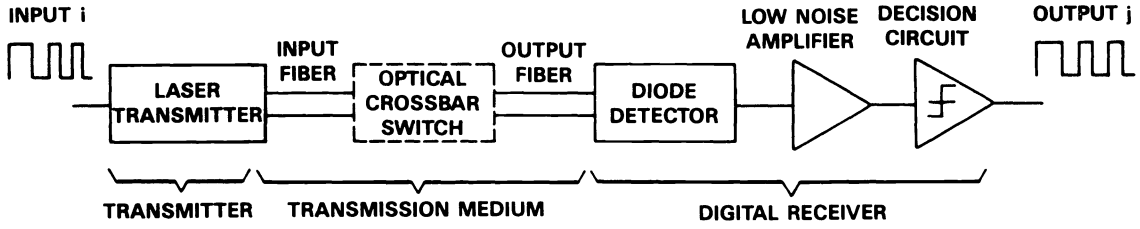

Fig. 3 Description of optical crossbar switch as a digital communications link.

occurs in the crossbar optics rather than the fiber. Semiconductor photodiodes can have noise-limited sensitivities of around 0.1 mW for direct detection of near-gigahertz binary signals. Semiconductor communications lasers are now capable of producing 10 to 30 mW of optical power.[7] In the analysis that follows, the ratio of optical power generated to power detected is considered to be the primary limiting factor to the number of channels N that an $N \times N$ crossbar switch will support.

Other noise sources are laser noise and dispersion in the transmission media, and these must be sufficiently small in order to approach the detector limited performance. Laser diodes have been measured[8] with relative intensity noise (RIN) of -120 to -160 dB/Hz. This is equivalent to a 30- to 70-dB (electrical) SNR in a 1-GHz bandwidth. These levels of laser noise are lower than the detection limit for a 10^{-9} bit error rate (21.5-dB SNR).[8,9] Dispersion is also quite small due to the system dimensions of the crossbar switch and the assumptions that the laser diodes used are single-mode longitudinal.[7] The transverse radiation pattern of these diodes is also a circularly symmetric, fundamental Gaussian mode, which allows efficient coupling to single-mode fiber guides.

3 Analysis of Loss and Contrast in Crossbar Optics

Several sources of loss, such as glass attenuation, metal reflectivity, and beamsplitter loss, were estimated using typical values from standard optics references. We assume that the light from a transmitter is shaped to nearly uniformly illuminate an N pixel row of the DMD. Uniform fanout reduces the intensity from a pixel by $1/N$. Light can be entirely captured by the vertical aperture of a row, but the space between pixels (equal to pixel width in this analysis) reduces light intensity per channel by another factor of 0.5. Three additional issues affect link performance and form

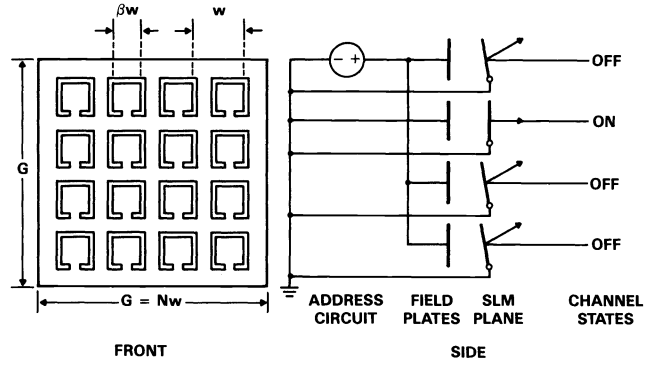

Fig. 4 The DMD: (a) reflective top surface and (b) side view of one column shown switching light. Dimensions for numerical calculation are assumed to be 50 μm for w and 0.5 for β.

the bulk of this discussion: (1) losses that arise from nonuniform illumination of rows of the DMD, (2) losses in illuminating finite aperture lenses, and (3) reduced contrast between on and off states due to stray light.

The last imaging lens (Fig. 2) forms the aperture that light will intercept in an on state and miss in the off state. The essentials of this limiting geometry are modeled by Fig. 5. Each DMD column is imaged onto its associated detector of width L_D with magnification

$$M = \frac{S_2}{S_1} = \frac{L_D}{NW} , \tag{1}$$

where L_D is assumed to be 70 μm, which is a typical size for high-speed, high-sensitivity detectors.[10,11] As long as the detector dark current and capacitance limit high-speed detectors to this size, significant demagnification from the DMD column to the detector is required. For this arrangement, light collection efficiency is influenced by the bundle

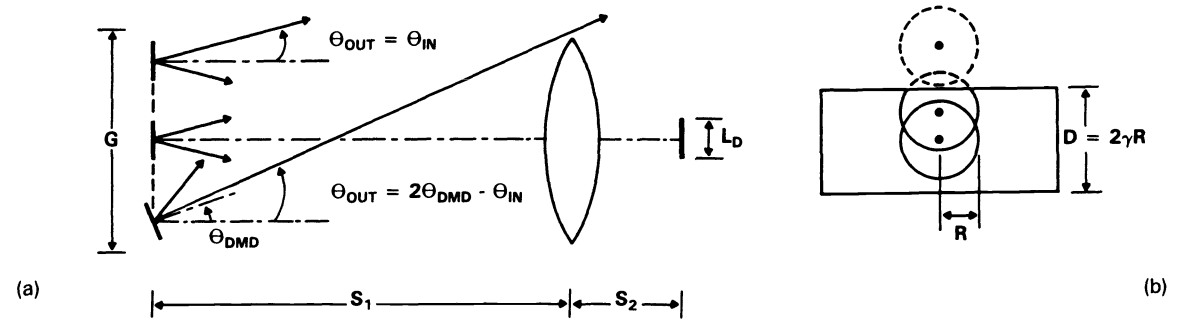

Fig. 5 Essential imaging geometry from DMD to detector: (a) side view and (b) transverse view of intersection of light bundles with collection lens. The incident bundle spread $2\theta_{IN}$ is assumed to equal approximately the exiting bundle spread $2\theta_{OUT}$ in this analysis.

spread off individual DMD mirror elements (pixels), the lens diameter D, and the width G of the SLM.

3.1 *DMD Mirror Element Deflection Requirements*

For complete removal of DMD-induced crosstalk due to the extreme pixel (as illustrated by the lower pixel in Fig. 5), a minimum deflection of θ_{DMD} is determined from the inequality

$$\frac{G+D}{2S_1} < 2\theta_{DMD} - \theta_{IN} \ , \tag{2}$$

where the left side describes (using the small-angle approximation) the minimum angle for θ_{OUT} needed for the bundle to miss the lens. If pixels deflect in opposite directions above and below the optical axis, the inequality can be further reduced to

$$\frac{D}{2S_1} < 2\theta_{DMD} - \theta_{IN} \ . \tag{3}$$

For low angular spread NA_{IN} will be used interchangeably with θ_{IN}. The relative aperture of the collection lens is conveniently represented by

$$NA_{LENS} = \frac{D}{2f} \ , \tag{4}$$

which is a small-angle approximation to actual numerical aperture $NA = \sin\theta$. The term NA_{LENS} will be used in this analysis even when it does not approximate NA well. In the case for which magnification M is much less than unity, then S_2 approximates the focal length f. Equation (3) can then be rewritten in terms of Eq. (4) as

$$\gamma = M\frac{NA_{LENS}}{NA_{IN}} < 2\left(\frac{\theta_{DMD}}{NA_{IN}} - \frac{1}{2}\right) \ . \tag{5}$$

Equation (5) shows that NA_{IN} must be limited to deflect all light outside the lens aperture. At minimum, θ_{DMD} needs to be 0.5 NA_{IN} (for $M = 0$). In current devices[6,12] θ_{DMD} is limited to around 0.12 radian, enabling a maximum allowable NA_{IN} of 0.24. Achieving light bundles with an NA_{IN} of less than 0.24 depends on the transmitter plane radiation characteristics, the lens transformation of the object plane to the DMD, and the diffraction of this image from the DMD surface. Since the bundle spread changes by $1/M$ from transmitter to DMD plane, it will be necessary to radiate from a small-diameter, low-divergence source. Using multimode fiber as a source would be unacceptable with current DMD dimensions.

Consider two examples. For commonly available multimode fibers, the lowest NA is around 0.2 and the smallest core is 50 μm. A magnification of 0.5 at most is required to image the entire core onto the pixel. This leads to an NA_{IN} of at least 0.4. This value is then too large to turn off the pixels. Single-mode cable is 0.1 NA with a less than 10-μm core diameter for typical laser diode sources (0.84 to 1.55 μm). With a core of less than 10 μm and 20-μm core-to-core spacing, a 2.5× magnification will map the bundle NA to 0.04 at the DMD plane, which can satisfy Eq. (5).

For a wavelength of 1 μm, the 0.04 NA incident bundle (treated as a circular Gaussian beam) would form a spot with a 99% energy encirclement diameter of 24 μm. (Because the beam is confined to a rectangular aperture of a DMD row rather than a circular aperture, there is even less clipping and energy loss.) This condition keeps diffraction from significantly broadening the angular spread of the light reflecting off the flap. For this reason, we have approximated the vertical bundle spread from the DMD with the incident bundle spread (as indicated on Fig. 5). (The bundle spread from individual pixels along the row is set by the diffraction caused by a uniformly, or very nearly uniformly illuminated, pixel.)

We just determined above that single-mode fiber will radiate the low-divergence illumination needed to switch individual pixels of the crossbar between on and off states. Is it also possible to make an array of single-mode sources for this application?

It is certainly possible to create fiber optic bundles with core-to-core spacing of 20 μm (e.g., Schott Fiber Optics manufactures fused fiber optic bundles from fibers of 4 to 50 μm in diameter.) However, this may not be practical in the case for which each transmitter is a discrete component and is connected to the crossbar input plane by an individual fiber optic cable. Small-diameter fibers are too easily broken in this situation. Single-mode fibers, used in long distance communications, are manufactured to a nominal diameter of 125 μm, which makes them highly reliable. For these fibers it is not possible to space fibers 20 μm apart. However, for the crossbar it is still possible to separate the single-mode sources *vertically* by this amount. The fiber bundle proposed in Fig. 6 serves this purpose. The horizontal stag-

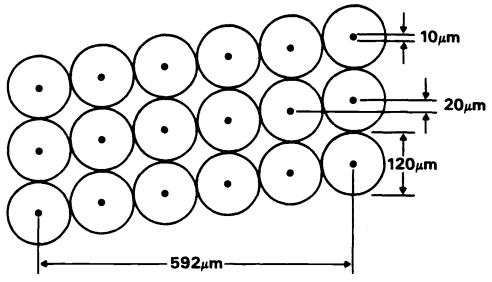

Fig. 6 Proposed single-mode fiber bundle with core vertical spacing to core diameter equal to DMD row separation to pixel width.

ger of the fibers will cause only small variations in the uniformity of illumination between rows of the DMD if the light is allowed to spread somewhat wider than the bundle width (as shown in the next section). Such a bundle would be constructed by stripping back the buffer layer at the end of each fiber (as is done in connectorizing fibers) and then gathering them together in a mechanical brace. In Fig. 6 the dimensions have been chosen to simplify the presentation. Using 125 μm as the exact dimensions of the cable, 20-μm vertical spacing can still be achieved. For example, a layer of seven fibers would have an end core-to-end core horizontal spacing of 740 μm and 120-μm spacing in the vertical. A 15.2-μm spacer placed between layers (i.e., a 15-μm offset in the vertical direction) would allow the next layer to begin 140 μm higher than the previous layer, and thus achieve the desired 20-μm spacing. There are other bundle layouts that would achieve the desired spacing, some of which can be handled by small changes in the source to DMD magnification.

3.2 *Row Illumination Efficiency*

The illumination of a DMD row is derived from a circular beam (see Fig. 7). The anamorphic lens set compresses the beam vertically. Thus the energy density at the end pixel will typically be smaller than at the central pixel. The uniformity of illumination is improved by increasing the beam radius, but this also wastes more light than before. To achieve the best energy utilization, the light available to the least illuminated pixel needs to be maximized.

An approximate analysis is used to illustrate these characteristics. The illumination will be treated as uniform out to a radius of R, and we assume that this model approximately represents the far-field pattern from a point source of small angular divergence. Figure 7 illustrates this geometry. The parameter γ compares the row length to the diameter of the source footprint. (Throughout this paper, γ compares the dimensions of source illumination to that of an aperture. In this section γ specifically refers to illumination of the DMD row, while in Secs. 3.1 and 3.3 γ refers to the illumination of the aperture of the N:1 imaging lens.) From the geometry of Fig. 7, the uniformity of row illumination is

$$U(\gamma)=(1-\gamma^2)^{1/2} \quad . \tag{6}$$

The ratio of light intercepted by a row to total illumination, or efficiency, would then be

$$E(\gamma)=\int_0^{\gamma} U(\alpha)\, d\alpha \quad , \tag{7}$$

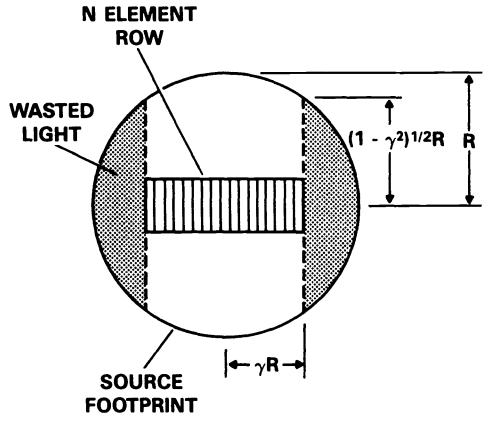

Fig. 7 Geometry in illuminating a row from a low-NA point source.

which evaluates to

$$E(\gamma)=\begin{cases}\frac{2}{\pi}[\gamma(1-\gamma^2)^{1/2}+\sin^{-1}\gamma] \quad , & \text{for } 0\leq\gamma\leq 1\\ 1 \quad , & \text{for } \gamma\geq 1\end{cases} \quad . \tag{8}$$

Equations (6) and (8) and their products are plotted in Fig. 8. Less than 2.5-dB overall loss is incurred for γ between 0.56 and 0.76. Since this curve has a broad valley, we can also see that the illumination variation due to a staggered bundle can be made small for a small bundle width. For the 600-μm bundle and pixel geometry discussed earlier, 2.5-dB overall loss would be achievable in crossbars as small as 40×40. Somewhat greater losses will be found by using intensity-weighted radial distributions for the beam profile[13] (e.g., the Gaussian distribution).

3.3 *Lens Collection Efficiency*

The results from the previous two sections can be applied to the formulation of lens collection efficiency. Section 3.1 established limits on bundle spread that led to low crosstalk. It can be seen, in Fig. 5, that low θ_{IN} is also desired for high collection efficiency from on-axis pixels. Lower θ_{IN} would actually diminish collection efficiency from extreme pixels if the DMD is of greater width G than vertical lens diameter D. Due to geometric similarities between DMD row illumination and illumination of a cylindrical lens, the mathematical results from Sec. 3.2 will be applied with only slight modification.

The intensity ratio of light intercepting the lens from the extreme pixel to light reflected from the pixel is our definition of lens collection efficiency. It is assumed that all light intercepting the lens is collected by the detector.

Two parameters can be used to describe all geometries illustrated in Fig. 5 for collection efficiency calculations. The parameter

$$C=\frac{G}{D} \tag{9}$$

normalizes DMD width to lens diameter while

$$\gamma=\frac{D}{2R} \tag{10}$$

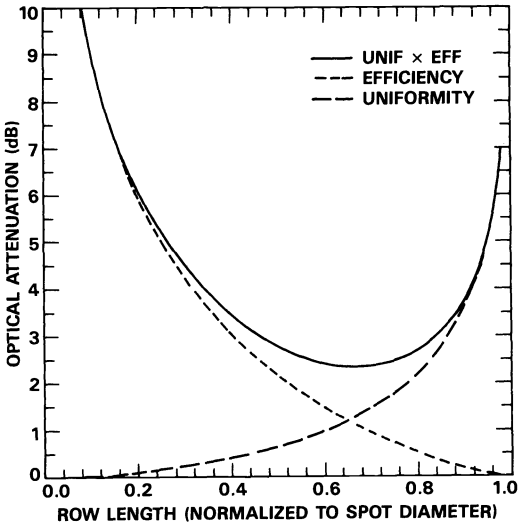

Fig. 8 Overall efficiency in illuminating a DMD row from a point source.

normalizes lens width to spot diameter at the lens.

If we again assume, as was done in Sec. 3.2, that the spot is a circle of uniform intensity, then Eq. (8) can be used to describe lens collection efficiency from the central pixel. This is seen by comparing Fig. 5(b) to Fig. 7 (rotated by 90 deg). Figure 5(b) shows the case where $E(\gamma)$ is unity. Since the collection efficiency from the end pixel will always be the lowest, the calculation for the overall efficiency needs to be modified. Equation (7) may be integrated over shifted limits or Eq. (8) can be applied to the upper and lower halves of the G/2 offset spot to yield

$$E(\gamma, C)=\begin{cases}\frac{1}{2}[E(\gamma+\gamma C)+E(\gamma-\gamma C)], & \text{for } 0\leqslant C\leqslant 1\\ \frac{1}{2}[E(\gamma+\gamma C)-E(\gamma C-\gamma)], & \text{for } C\geqslant 1\end{cases} \tag{11}$$

Figure 9 plots Eq. (11) against C. For large γ the central spot underfills the lens. As DMD width increases, the extreme spot moves outside the lens aperture. Because the spot diameter is small compared to the lens aperture, the curve transitions rapidly from unity to zero efficiency. For small γ the central spot overfills the lens and accounts for most of the loss. Efficiency becomes nearly independent of C (over this range) because the extreme spot has an almost rectangular overlap of nearly the same dimensions as the central spot. In the small γ region, efficiency can also be seen to be independent of C, as well as asymptotically linear in Fig. 10. In this region

$$E(\gamma, C)\simeq\frac{4}{\pi}\gamma \ . \tag{12}$$

For larger γ each curve has a unique "saturation" characteristic. Most notable is the $C=1$ curve, which has a constant saturated efficiency of 0.5. [This region is also represented by the point (1, 0.5) in Fig. 9.] Here, as illustrated in the legend, the extreme pixel and the lens edge are at the same elevation. For increasing C, the spot centerline is above the lens edge. This results in increasing losses as the spot width decreases with respect to the lens.

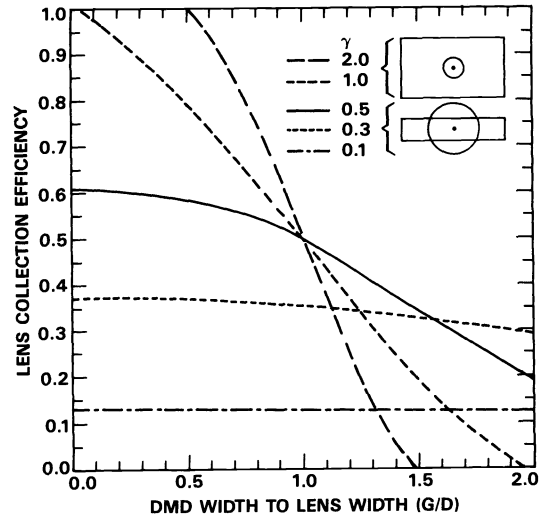

Fig. 9 Overall lens collection efficiency.

The asymptotic form of lens collection efficiency, Eq. (12), if set to unity can be used to estimate the size N_o of a crossbar switch for which the illumination just begins to overfill the lens. For decreasing γ, efficiency approaches

$$E(\gamma, C)=\frac{N_o}{N} \ , \tag{13}$$

where N_o serves as a breakpoint between unit efficiency and efficiency that decreases proportional to $1/N$. A value for N_o of 89 results for $L_D=70$ μm, $w=50$ μm; $\mathrm{NA_{IN}}=0.04$, and $\mathrm{NA_{LENS}}=2$, while a value for N_o of 32 results for L_D and $\mathrm{NA_{LENS}}$ changed to 100 μm and 0.5, respectively (which would be appropriate if the detectors are fiber coupled).

3.4 *Open-Air Versus Fiber Detector Coupling Efficiency*

Either an open-air detector array or a fiber bundle connected to discrete detectors can be placed in the receiving plane. Detector arrays offer the advantages of large acceptance angle and compact integration compared to discrete receivers. However, they cannot as yet meet the sensitivity and immunity to electrical crosstalk possible with discrete detectors.[14,15] Making a large number of off-chip connections for numerous high-bandwidth signals also appears to require substantial manufacturing art. For these reasons, implementations of both forms are considered.

Fiber optics has a finite acceptance angle described by NA_f. For the typical case with M much less than 1, the maximum effective $\mathrm{NA_{LENS}}$ is limited to NA_f. The fiber has a core diameter D_f that is different from L_D. This leads to a comparison of efficiency between the two implementations:

$$\frac{E_f}{E_d}=\left(\frac{D_f}{L_D}\frac{NA_f}{NA_{\mathrm{LENS}}}\right)\left(\frac{L_D}{D_f}\right)^2 \ . \tag{14}$$

The first group of terms uses Eq. (12) to compare coupling efficiency into a fiber to coupling efficiency directly into a detector. The second term is a rough estimate of coupling efficiency at a "pigtailed" fiber/detector interface. Of standard available fiber optic cable known to us, 0.5-NA 100-μm-

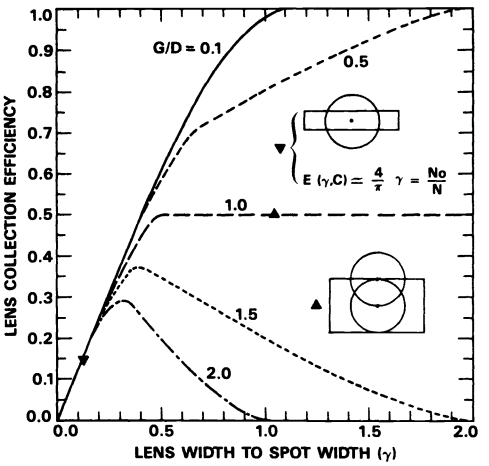

Fig. 10 Overall lens collection versus C.

diam core maximizes Eq. (14). (Since this fiber has a total diameter of 140 μm, the image of the DMD rows would be magnified by a minimum of 2.8× in the horizontal direction in order to overlay a single row of receiving fibers.) An NA_{LENS} of 2 (which is equivalent to 0.89 NA) is chosen as the maximum for the detector array configuration. This value is achieved in the design of standard microscope objectives.

4 System Dimensions and Signal Dispersion

For large switch size N, the distance between the DMD and the collection lens can become the dominant length of the optical system. Because good collection efficiency and uniformity of collection is required, the lens diameter can also be wide enough to cause noticeable delays in propagation between on- and off-axis rays. The geometric model of the crossbar optics will be used to estimate the significance of these parameters.

For large N the length is approximated as

$$L=\frac{f}{M}=\frac{(Nw)^2}{2CL_D\mathrm{NA}_{\mathrm{LENS}}}\ , \tag{15}$$

where Eqs. (1), (9), and (10) along with $G=Nw$ have been used. On-axis delay is roughly

$$t=\frac{L}{v} \tag{16}$$

where v is the speed of light. Total dispersion Δt is due primarily to the extra path length from the edge of the collection lens to the detector and is

$$\Delta t=tM[(1+\mathrm{NA}_{\mathrm{LENS}}^2)^{1/2}-1]\ . \tag{17}$$

Table 1 gives some results for typical crossbar sizes. Several observations can be made. The system length can become quite large for large N since L grows at a quadratic rate. Section 3.3 showed, however, that for large switch sizes, C is nearly independent of collection efficiency. Thus, C can be used as a design parameter to achieve a desirable switch size with adequately low dispersion. For example, 78-ps dispersion leads to a 1-dB receiver sensitivity loss at 3.2 Gb/s transmission rates.[16] For a 1000×1000 crossbar this limit could be met with up to a 41-mm lens.

Table 1 Dimensions and delay in crossbar optics.

Switch Size	L (M)	D (mm)	f (mm)	t (ns)	Δt (ps)
N	9×10^{-6} N^2/C	0.05 N/C	0.013 N/C	30×10^6 N^2/C	.094 N/C
128	0.15/C	6.4/C	1.6/C	.49/C	12/C
512	2.4/C	26/C	6.4/C	7.9/C	48/C
1000	9/C	50/C	12.5/C	30/C	94/C

Note: NA_{lens} = 2, L_D = 70 μm, w = 50 μm

5 Energy Budget of Optical Crossbar

Table 2 contains estimates for the significant terms in the energy budget. The last two terms are considered lossless. Transverse single-mode lasers with circularly symmetric radiation profiles can ideally be lens coupled to single-mode fibers with no loss if precise alignment and magnification are maintained. (The achievement of near-lossless laser to fiber coupling is primarily determined by the engineering and manufacturing costs involved.) Overfill of the DMD pixel was discussed in Sec. 3.1. Further discussion of the parameters in Table 2 are found in Ref. 13.

The individual terms may be combined to yield the overall power available at the detector:

$$P_{\mathrm{AVL}}=\frac{0.034}{N}\frac{N_o}{N}\left(\frac{L_D}{D_f}\right)^2 P_{\mathrm{IN}}\ , \tag{18}$$

where Eq. (13) is used to simplify $E(\gamma, C)$. The value of P_{AVL} must be no smaller than P_{MIN}, the minimum detectable power level for a specified bit error rate (BER).[9]

Equation (18) is examined for the three receiver types detailed in Table 3. Equation (18) is normalized by P_{MIN} and plotted in Fig. 11. The first three curves decay at a $1/N$ rate before the lens is filled and $1/N^2$ after the lens is filled. Using the commercially available case i receiver a 300×300 crossbar is possible at 320 Mb/s. The case ii receiver performance is based on projections of future device performance and the incorporation of such devices into receiver arrays. Crossbars using this receiver appear to have a maximum size of 850 at 3.2 Gb/s. Quantum limited performance is also included for reference.

The two other curves in Fig. 11 are included to illustrate the effect of crosstalk on switch size. These curves represent sensitivity derating due to equal contribution of light, C_t below the on pixel intensity, from $N-1$ off pixels. The curves only include the effect of uncertain threshold and do not consider crosstalk-generated shot noise. The intersection of the derating curve with the energy budget limits the switch size to approximately

$$N_{\mathrm{MAX}}=\frac{1}{C_t} \tag{19}$$

if pixel-induced crosstalk is substantially larger than P_{MIN}. Depending on a particular switch geometry, each pixel may instead contribute differing amounts to crosstalk. Further theoretical and experimental analysis of scattering is required to determine reasonable bounds on crosstalk and stray light.

Table 2 Terms included in crossbar energy budget.

Variable	Symbol	Ranges
Switch Size	N	1-10,000
Transmitter Power	P_{in}	30 mW
Detector Sensitivity for 10^{-9} BER	P_{min}	2.2×10^{-6} to 1.8×10^{-4} mW
Spread Across Row		1/N
Demagnification to Detector	E(γ,C)	32/N to 89/N
Fiber to Detector Pigtail	$(L_D/D_f)^2$	.49 to 1
Spread Wider than Row	E	.55
Beam Splitter		.25
Undeformable Surface		.5
Fiber and Splice Loss		.65
AR Coated Glass		.85
Pixel Reflectivity		.90
Transmitter to Fiber		1
Vertical Overfill of Pixel		1

Table 3 Summary of receiver attributes used in analysis.

Case	Detector	Wavelength (μm)	Data Rate (Gbs)	Detection Method	Sensitivity (mW)	Detector Coupling
i	PinFet[17]	1.3	.32	Direct NRZ	1.78×10^{-4}	pigtail
ii	APD[18]	1.55	3.2	Direct NRZ	1.26×10^{-4}	Open air
iii	----	1.3	3.2	Homodyne PSK[19]	2.20×10^{-6}	Open air

6 Conclusions

The DMD-based crossbar will require careful control of coherent light to approach its maximum size. Certain geometric relations between bundle spreads and apertures must be obtained for a crossbar to even begin to work. With these conditions, we see that approaching the estimated performance limits will require state-of-the-art transmitters and receivers, and new fiber bundle manufacturing techniques, not to mention large-area spatial light modulators. Efficient light utilization and low distortion across a wide field of view also necessitate involved lens designs. The model presented will help to focus appropriately on further modeling and experimental confirmation of the crossbar characteristics. At the same time, with the fundamental principles understood, computer-aided optical design packages can be intelligently applied to design and specification of realistic optics and to rigorous analysis of prototype crossbars.

Acknowledgments

This work was supported in part by the Defense Advanced Research Projects Administration through Office of Naval Research contract N00014-85-C-0755 and the Bell South Foundation from a grant through the South Central Bell/ University of Louisville Telecommunications Research Center.

References

1. A. D. McAulay, "Optical crossbar interconnected digital signal processor with basic algorithms," *Opt. Eng.* **25**(1), 82–90 (1986).
2. P. R. Haugen, S. Rychnovsky, A. Husain, and L. D. Hutcheson, "Optical interconnects for high speed computing," *Opt. Eng.* **25**(10), 1076–1085 (1986).
3. F. A. Tobagi, "Fast packet switch architectures for broadband integrated services digital networks," *Proc. IEEE* **78**(1), 133–167 (1990).
4. A. Himero and M. Kobayashi, "4 × 4 optical-gate matrix switch," *J. Lightwave Technol.* **LT-3**(2), 230–235 (1985).

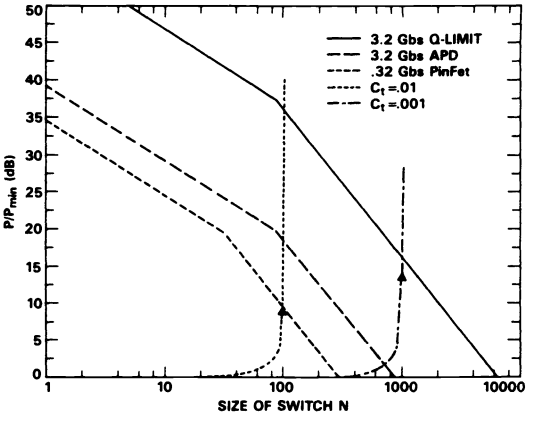

Fig. 11 Link energy budget of optical crossbar versus switch size.

5. D. G. Grant, R. A. Meyer, and D. N. Qualkinbush, "An optical phased array beam steering technique," *1971 Proc. Electro Optic System Design Conf.*, New York, September 1971, pp. 259–264.
6. D. A. Gregory, R. D. Juday, J. Sampsell, R. Gale, R. W. Cohn, and S. E. Monroe, Jr., "Optical characteristics of a deformable-mirror spatial light modulator," *Opt. Lett.* **13**(1), 10–12 (1988).
7. Ortel Corporation, 2015 W. Chestnut Street, Alhambra, CA 91803.
8. G. Keiser, *Optical Fiber Communications*, 2nd ed., pp. 361–365, McGraw Hill, New York (1991).
9. A. Yariv, "Detection of optical radiation," in *Introduction to Optical Electronics*, 2nd ed., Chap. 11, pp. 298–336, Holt, Rinehart, and Winston, New York (1976).
10. R. S. Sussman, R. M. Ash, A. D. Mosely, and R. L. Goodfellow, "Ultra-low capacitance flip chip bonded GaInAs pin photodetector for long wavelength high data rate fibre optic systems," *Electron. Lett.* **21**(14), 593 (1985).
11. M. Ito and O. Wada, "Low dark current GaAs metal semiconductor metal (MSM) photodiodes using WSi_x contact," *J. Quantum Electron.* **QE-22**(7), 1073 (1986).
12. R. W. Cohn and J. B. Sampsell, "Deformable mirror device uses in frequency excision and optical switching," *Appl. Opt.* **27**(5), 937–940 (1988).
13. D. W. Oxley, A. D. McAulay, R. W. Cohn, J. D. Provence, E. Parsons, and D. Casasent, "Final report: optical crossbar interconnected signal processor," DARPA No. N00014-85-C-0755 (May 1987).
14. D. R. Kaplan and S. R. Forrest, "Electrical crosstalk in p-i-n arrays part I: theory," *J. Lightwave Technol.* **LT-4**(10), 1460 (1986).
15. M. G. Brown, P. H-S Hu, D. R. Kaplan, Y. Ota, C. W. Seabury, M. A. Washington, E. E. Becker, J. G. Johnson, M. Koza, and J. R. Potpowicz, "Monolithically integrated 1 × 12 array of planar InGaAs/InP photodiodes," *J. Lightwave Technol.* **LT-4**(3), 283 (1986).
16. Technical Staff Members, "Optical fibers transmission systems," in *Transmission Systems for Communications*, Bell Telephone Laboratories, Chap. 34, pp. 821–840 (1982).
17. Plesscor Optronics, 20200 Sunburst St., Chatsworth, CA 93133-6289.
18. R. C. Goodfellow, B. T. Debney, J. R. Graham, and J. Buus, "Optoelectronic components for multigigabit systems," *J. Lightwave Technol.* **LT-3**(6), 1170–1179 (1985).
19. E. Basch and T. Brown, "Introduction to coherent fiber-optic communication," in *Optical-Fiber Transmission*, E. Basch, Ed., p. 521, Howard W. Sams and Co., Indianapolis (1987).

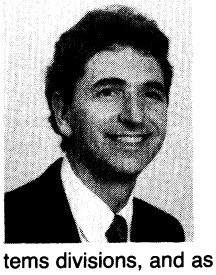

Robert W. Cohn received the Ph.D. in electrical engineering from Southern Methodist University, Dallas, in 1988. He is an associate professor at the University of Louisville in the Department of Electrical Engineering where he is pursuing research on optical and acoustic information processing. From 1978 to 1989 he was with Texas Instruments as a member of the technical staff (1984–89) in the Central Research Laboratories and the Defense Systems divisions, and as a design engineer (1978–83) in the Defense Systems division. His research there included compensation of second-order effects in SAW filters, optical processing using deformable mirrors, image processing algorithms, and the development of microwave hybrid components. Cohn is a senior member of IEEE and a member of SPIE.